Synchronization of bursting Hodgkin-Huxley-type neurons in clustered networks

T. de L. Prado,[1,2,4] S. R. Lopes,[1] C. A. S. Batista,[1] J. Kurths,[2,3,4] and R. L. Viana[1,*]

[1]*Departament of Physics, Federal University of Parana, Caixa Postal 19044, 81531-990, Curitiba, Paraná, Brazil*
[2]*Institute of Physics, Humboldt University, D-10099 Berlin, Germany*
[3]*Institute for Complex Systems and Mathematical Biology, Aberdeen, AB243UE, United Kingdom*
[4]*Potsdam Institute for Climate Impact Research, P. O. Box 601203, 14412 Potsdam, Germany*

We considered a clustered network of bursting neurons described by the Huber-Braun model. In the upper level of the network we used the connectivity matrix of the cat cerebral cortex network, and in the lower level each cortex area (or cluster) is modelled as a small-world network. There are two different coupling strengths related to inter- and intracluster dynamics. Each bursting cycle is composed of a quiescent period followed by a rapid chaotic sequence of spikes, and we defined a geometric phase which enables us to investigate the onset of synchronized bursting, as the state in which the neuron start bursting at the same time, whereas their spikes may remain uncorrelated. The bursting synchronization of a clustered network has been investigated using an order parameter and the average field of the network in order to identify regimes in which each cluster may display synchronized behavior, whereas the overall network does not. We introduce quantifiers to evaluate the relative contribution of each cluster in the partial synchronized behavior of the whole network. Our main finding is that we typically observe in the clustered network not a complete phase synchronized regime but instead a complex pattern of partial phase synchronization in which different cortical areas may be internally synchronized at distinct phase values, hence they are not externally synchronized, unless the coupling strengths are too large.

I. INTRODUCTION

In the brain neurons are connected through synapses and comprise a complex network, due to both the large number of nodes ($N \sim 10^{11}$ cells) as well as the large connectivity (each neuron is linked to $\sim 10^4$ others, with $K \sim 10^{15}$ links) [1]. However, there are several description levels in which we can investigate complex anatomical networks in the brain. In a microscopic level we consider the neurons as nodes and their synaptical connections as links [2]. However, at a macroscopic level areas of the cerebral cortex can be taken as nodes, the corresponding links being axonal fibers connecting neurons from different cortical areas [3]. There are also functional networks, for which the nodes are cortical areas as well, but the links are determined from correlations between such areas when the subject performs a given function. This is currently done by using medical imaging [4].

There are some neuroanatomic networks which have been intensively studied in the past several years which have served as paradigmatic models for computer simulations of neuronal networks. One of them is the cat cerebral cortex, consisting of $N = 53$ cortical areas, connected through $K = 826$ directed links [5]. These cortical areas are organized into four classes according to their common functionality: visual, auditory, somatosensory-motor, and frontolimbic [6,7]. Each cortical area is a network itself formed by neurons connected through electrical and chemical synapses. Hence a proper description of the cat cortex would be a network of networks or clustered network [8].

In this case, each cortical area is regarded as a network of neurons interacting with neurons from the same cortical area as well as from others. Many different connection architectures for clustered networks have been considered. One of them considers each cortical area as a small-world network in which, from the N neurons belonging to each area, 30–40% of them are connected with neurons belonging to different areas [9]. This can be modelled as a random network characterized by an intercluster probability ("random-plus-small-world"). Another connection architecture regards each cortical area as a scale-free network, in which there is a highly connected hub. These richly connected hubs interact through a globally coupled network ("rich club") [10].

In this paper we propose a different architecture for clustered networks based on the cat cortical connectivity matrix, where each cortical area is modelled by a small-world network of individual neurons. Instead of considering the synapses among neurons belonging to different cortical areas, we make the hypothesis that the cortical areas interact through their mean fields. In other words, we assume that the axonal fibers connecting two cortical areas are represented by a coupling between the corresponding microscopic mean fields. This is actually a coarse-grained description of neuron activity and is expected to hold as long as we regard each cortical area as producing a coherent membrane potential. Hence, we expect the neurons from each cortical areas to act synchronously to generate a coherent signal which is represented by the mean field.

One intensively investigated type of synchronization in neuronal networks is synchronization of bursting behavior [11]. The latter is characterized by groups of fast spikes with subsequent quiescent behavior, i.e., there are two time scales: fast (spiking) and slow (bursting) [12]. It is known that practically any neuron can exhibit bursting if stimulated or pharmacologically manipulated in a convenient way. Bursting behavior is crucial in neuronal communication. In particular, in a burst of many repeated spikes the excitatory postsynaptic potentials of each spike are added, facilitating the production

---

*Corresponding author: viana@fisica.ufpr.br

of suprathreshold potentials [13]. Moreover, bursts are all-or-nothing events, in the sense that some individual spikes may be due to noise, whereas bursts of spikes are robust events with respect to noise [14].

Neurons described by Hodgkin-Huxley equations spike due to the interplay between fast sodium and potassium currents [15]. Such neurons exhibit bursting due to slow calcium currents that modulate spiking activity. Other models, however, are based on Hodgkin-Huxley-type thermally sensitive neurons [16–18], which describe spike train patterns experimentally observed in facial cold receptors and hypothalamic neurons of a rat [19], electroreceptors organs of freshwater catfish [20], and caudal photoreceptor of a crayfish [21]. There have been studied time delay- and coupling strength-induced synchronization transitions in scale-free networks of thermally sensitive neurons [22]. The synchronous behavior of two coupled thermally sensitive neurons has been numerically investigated as a function of the coupling strength, exhibiting a transition between a tonic firing to a bursting behavior [23].

Synchronization properties of complex networks have been investigated in depth by many authors, particularly the issue of complete synchronization, for which the coupled dynamical units attached to the network nodes have identical dynamical behavior [24]. In the case of spiking neurons, complete synchronization would mean coincidence of spiking events [11]. Bursting synchronization, however, does not require spiking to occur at the same times and can be more properly classified as phase synchronization [25]. Phase synchronization in clustered networks has been studied from the point of view of its applications in neuronal networks, particularly the "rich club" [10] and "random-plus-small-world" [26] models. Another type is frequency synchronization, for which only the time rates of the phase evolution are taken into account [27].

Networks of heterogeneous networks have been described as communities of several distinct populations. In neuroscience this can describe populations of excitatory and inhibitory neurons and glia, for which global behavior can be observed when the natural frequencies are randomly distributed according to a given distribution [28]. Other dynamical behaviors have been found when the coupling functions are asymmetric, such as bistability and higher-order entrainment [29]. The case of heterogeneous coupling between the subpopulation of such a clustered network has shown to lead to quasiperiodic chimera states [30]. The issues of local and global synchronization have been studied in modular networks with heterogeneous frequencies, and transitions between these states can be observed varying the relative strength of local and global coupling strengths [31,32].

In this paper we aim to investigate bursting synchronization in a clustered network in which the outer level consists of the cat cerebral cortex network, as known in the literature [5,6], and the cortical areas (inner level) are a small world of bursting neurons [33,34]. The coupling in the outer level is performed among the mean field of the networks representing each cortical area. The dynamics of the latter is described by the Huber-Braun (HB) model of Hodgkin-Huxley-type thermally sensitive neurons [16]. Many previous works on this model have focused on the properties of individual neurons or assemblies of a few neurons. Networks of coupled Huber-Braun neurons have begun to be investigated only recently:

Phase synchronization of bursting HB neurons in small-world networks and its control have been recently described using chemically coupled neurons [35]. In the present work we report a numerical investigation of HB neurons in a clustered network structure.

One of the distinctive properties of clustered networks is that, while subnetworks (at the inner level) may exhibit bursting synchronization, the network as a whole (at the outer level) may be far from being synchronized. In fact, synchronization of the entire network is unlikely to occur, since it would represent an undesirable collective behavior for the brain. Hence it is worthwhile to consider partial synchronization of the clustered network in order to understand for which parameter intervals it may occur. Moreover, knowing how synchronization sets in for a complex network provides clues as how to control or even suppress it. In particular, there is compelling empirical evidence that pathological rhythms, like Parkinson's disease and essential tremor, are related to synchronized behavior in regions of the brain cortex [36–41]. Hence the control of synchronization in such conditions is potentially important to design proper ways to apply control strategies, like deep brain stimulation [42].

The rest of the paper is organized as follows: in Sec. II we present the model of a clustered network based on the cat cortical connectivity. Section III outlines the neuron bursting dynamics model used in the numerical simulations and the definition of a bursting phase. Section IV presents the model of a coupled neuronal assembly with a clustered connectivity. Section V deals with quantitative characterization of synchronized bursting through the different definitions of an order parameter and the average field of the network. Our conclusions are presented in the last section.

II. CONNECTION ARCHITECTURE OF THE CLUSTERED NETWORK

One of the systems for which the anatomic connectome has been extensively studied over the past two decades is the cat cerebral cortex, for which information from the neuroanatomical literature reporting anatomical tract-tracing experiments has been collected and organized by Scannell and coworkers [5–7]. In this data set the cat cerebral cortex has been divided into $N = 53$ cortical areas interconnected by $K = 826$ directed links representing fibers of axons. The overall density of links (i.e., the ratio between the number of links L and the total number of possible directed links connecting N nodes without self-interactions) is thus $\rho = K/N(N-1) \approx 0.3$ [34].

The corticocortical connectivity of the cat can be summarized by the weighted adjacency matrix $A = ((A_{ij}))$, depicted in Fig. 1, where the 53 cortical areas are identified by their anatomical abbreviations and the weights are assigned according to the axonal density of the fiber projections [8]. Hence a zero weight ($A_{ij} = 0$) means that the two cortical areas are not connected at all, otherwise they are connected in three levels of intensity: $A_{ij} = 1,2,3$. The diagonal elements A_{ii} vanish, since we do not consider self-interactions of cortical areas. Because the connections are directed (even though two areas may be connected where the weights in both
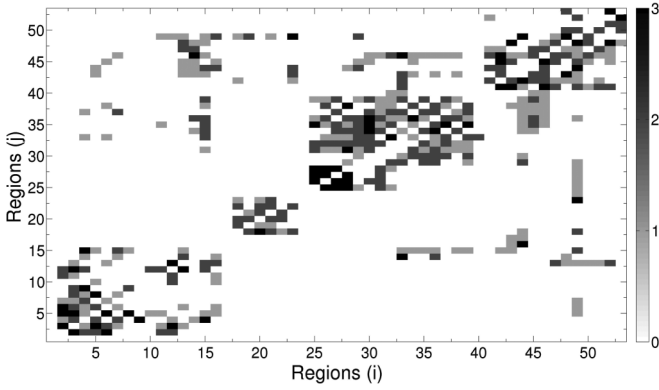
FIG. 1. Matrix representation of the corticocortical connectivity of the cat, according to Ref. [8]. The connections among cortical areas are classified as null (white), weak (light gray), intermediate (dark gray), and strong (black), with respect to the axonal density of fiber projections.

directions may differ), the adjacency matrix A is not expected to be symmetric at all.

The cortical areas are organized into four modules with common functional roles, namely the visual, auditory, somatosensory-motor, and frontolimbic. The four modules are groups of cortical areas classified by their overall role and form diagonal blocks in the matrix whose elements are internal connections, whereas the elements of off-diagonal blocks stand for the connections among different modules. Figure 1 reveals that the block-diagonal matrices representing the moduli are quite dense, whereas the off-block-diagonal parts are rather sparse.

There is an extensive literature on the quantitative characterization of complex networks [43]. For the sake of our purposes in this paper it suffices to consider two basic quantities: the average path length L and the average clustering coefficient C. The former is obtained by considering the minimum path length, measured in number of links, between two nodes in the network. L is obtained by averaging this path length over all distinct pairs of nodes. The clustering coefficient is given by $C = 3N_{tri}/N_{con}$, where N_{tri} is the number of triads of nodes completely connected among themselves and N_{tri} is the number of partially connected triads [44].

A type of network for which a great deal of useful mathematical properties are known is the random, or Erdös-Renyi (ER), network [45]. From a number N of initially disconnected nodes we build links between pairs of randomly chosen nodes with a uniform probability p_{rand}. When considering a complex network with N nodes and K links, and without self-interactions, we can define an equivalent random network with the same number of nodes and links, such that $p_{rand} = \rho$.

For an ER network we have $L_{rand} \sim \ln N / \ln[(K/N) - 1]$, i.e., it is small, since it increases slowly with the network size. The corresponding clustering coefficient is $C_{rand} \sim K/N^2$, and decays very rapidly with the network size. Small-world networks have small average path lengths, of the same order as in random networks, $L \sim L_{rand}$, but their average clustering coefficients are relatively large, $C \gg C_{rand}$ [27]. From the ratios $\lambda = L/L_{rand}$ and $\gamma = C/C_{rand}$ it is possible to define a merit figure $\sigma = \gamma/\lambda$ [33,34]. For a small-world network it yields $\sigma > 1$.

The cat cerebral cortex network has $L = 1.81$ and $C = 0.55$, such that the ratios are $\lambda = 1.06$, $\gamma = 1.77$, and the merit figure is $\sigma = 3.22$, thus indicating that this network has some small-world property [33,34]. Just for comparison, the connectome of *Caenorhabditis elegans*, which is usually given as an example of small-world network, has $\sigma = 14$ for the electric synapses, 2.78 for the chemical synapses, and 2.38 for the combined network [46]. Other networks, of both neuroanatomic and neurofunctional nature, have been observed to be of small-world type. Hence, for the inner level of the clustered network, there are good arguments to assume that each cortical area is a small-world network of individual neurons.

In order to get a small-world network, we have at our disposal two basic schemes: Watts-Strogatz (WS) and Newman-Watts (NW). WS networks are obtained from a one-dimensional chain of nodes with 2ℓ local connections, i.e., between ℓ neighbors at each side [47]. In this chain a number of links is randomly rewired with a probability p, such that in the limit $p \to 1$ we obtain an ER network. Hence the number of links in a NW network is $K = (2\ell + p)N$.

The WS procedure may lead to disconnected pieces in the network, hence we have chosen the NW network instead, for which the links are added, instead of rewired, with the same probability p [48]. As long as p is small enough, the two procedures yield similar results. However, in the limit $p \to 1$ a NW network will result in a densely connected network.

The small-world networks for each cortical area were obtained from the Newman-Watts procedure. We have chosen, as a reference value, a probability $p^* = 0.0001$, for which we found that the average path length is $L(p^*) = 25.7$ and the average clustering coefficient is $C(p^*) = 0.31$. Moreover, each network was obtained for a shortcut probability $p = 0.01$: From Fig. 2 we have $L(0.01) = 0.13L(p^*) = 3.34$ and $C(0.01) = 0.62C(p^*) = 0.31$. Since each network has $N = 256$ neurons, each of them in a chain with $\ell = 2$ neighbors at each side and pN nonlocal shortcuts, the total number of connections is $K = (2\ell + p)N \approx 1026$. In order to check the validity of the small-world approximation in this case we consider an equivalent random (ER) network, with the
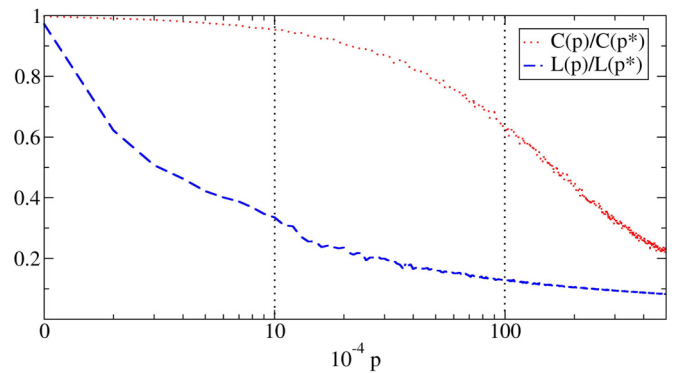

FIG. 2. (Color online) Normalized values of the average path length (dashed blue) and clustering coefficient (dotted red) as a function of the probability of nonlocal shortcuts for a Newman-Watts network of $N = 256$ nodes. The dotted vertical lines indicate the region where the small-world property is well expressed.

same number of nodes and links, and which has $L_{\text{rand}} = 5.04$ and $C_{\text{rand}} = 0.0156$ according to the expressions presented in Sec. II. Hence the ratios are

$$\lambda = \frac{L}{L_{\text{rand}}} = 0.663, \qquad \gamma = \frac{C}{C_{\text{rand}}} = 19.9,$$

from which we compute the merit figure $\sigma = \gamma/\lambda \approx 30$, which confirms our assumption of a network with the small-world property. In principle, since the latter requirement is rather weak (it suffices that $\sigma > 1$) we could have chosen a smaller probability. In fact, any value of p within the interval $[0.001, 0.01]$ could suit us well (this interval is indicated by dotted vertical lines in Fig. 2). However, a too-low value of p would require a correspondingly large network to yield good statistics for the averages. On the other hand, a too-large value of p would take us out of the interval for which the small-world property holds. This is the reason we have chosen $p = 0.01$ instead of other value. However, as long as we do not stray much apart from this value of p our results would not change qualitatively.

The small-world network so obtained can be described by an adjacency matrix $A = ((A_{ij}))$, where $A_{ij} = 1$ if two neurons are connected and $A_{ij} = 0$ otherwise. The diagonal elements are also zero since we did not take into account self-interactions. We did not assign weights to these inner couplings, because each cluster will contribute through its mean field, and thus the information about the network is averaging out the details of the connection architecture.

III. BURSTING NEURON DYNAMICS

In this section we describe briefly the equations and parameters of the HB model for thermally sensitive neurons [16,17,21]. The dynamics of the membrane potential V of the neuron is governed by the membrane equation (V is measured in mV and time in ms),

$$C_M \frac{dV}{dt} = -I_{\text{Na}} - I_K - I_{\text{sd}} - I_{\text{sa}} - I_L + I_{\text{ext}}, \quad (1)$$

where C_M is the membrane capacitance (measured in $\mu\text{F/cm}^2$). The current densities due to the sodium, potassium, and leak channels are denoted respectively by I_{Na}, I_K, and I_L (measured in $\mu\text{A/cm}^2$). The external current density I_{ext} is either injected or due to the synaptic coupling with other neurons.

The fast currents I_{Na}, I_K, and I_L are essentially the same as in the Hodgkin-Huxley (HH) model and are responsible for the production of action potentials. The key difference between the HB and HH models is the presence of two additional currents: I_{sd}, which refers to intrinsic subthreshold oscillations, and I_{sa}, related to hyperpolarization oscillations. Both I_{sd} and I_{sa} are slow currents responsible for the subthreshold activation, i.e., they activate the neurons more slowly when the membrane potentials are lower than the spiking threshold, and the interplay between fast and slow dynamics ultimately leads to a bursting [16].

It is possible to draw a parallelism between the HB model and those models using calcium SK channels (the so-called small conductance Ca^{2+}-activated K channels) [49,50]. The latter allow the passage of K ions through the neuron

membrane and are activated by an increase of the intracellular Ca^{2+} concentration. In this parallelism the combination of the currents I_{sd} and I_{sa} play the role of Ca^{2+} channels sensitive to the membrane potential. The difference is that SK channels are activated by the presence of Ca^{2+} ions, whereas I_{sd} and I_{sa} are activated by the membrane potential. This procedure of replacing an ion-sensitive to a voltage-gated channel is common in biophysical models of neurons, e.g., the inactivation of fast Na^+ channels is not really voltage gated, but it is modeled this way in many models of neuronal dynamics.

We associate a given ohmic conductance to each ion current, as

$$I_{\text{Na}} = \rho \bar{g}_{\text{Na}} a_{\text{Na}} (V - E_{\text{Na}}), \quad (2)$$

$$I_K = \rho \bar{g}_K a_K (V - E_K), \quad (3)$$

$$I_{\text{sd}} = \rho \bar{g}_{\text{sd}} a_{\text{sd}} (V - E_{\text{sd}}), \quad (4)$$

$$I_{\text{sa}} = \rho \bar{g}_{\text{sa}} a_{\text{sa}} (V - E_{\text{sa}}), \quad (5)$$

$$I_L = \rho \bar{g}_L (V - E_L), \quad (6)$$

where $\bar{g}_{\text{Na}}$, $\bar{g}_K$, $\bar{g}_{\text{sd}}$, $\bar{g}_{\text{sa}}$, and $\bar{g}_L$ are the maximum specific conductances (measured in mS/cm^2) and the reversal (Nernst) potentials for each ionic current are denoted by E_{Na}, E_K, E_{sd}, E_{sa}, and E_L. The parameter ρ is a scale factor depending on the temperature T, given by

$$\rho = \rho_0^{\frac{(T - T_0)}{\tau_0}}, \quad (7)$$

where ρ_0, T_0, and τ_0 are constants.

The time evolution of the activation currents a_{Na}, a_K, a_{sd}, and a_{sa} are governed by the following equations:

$$\frac{da_{\text{Na}}}{dt} = \frac{\phi}{\tau_{\text{Na}}} (a_{\text{Na},\infty} - a_{\text{Na}}), \quad (8)$$

$$\frac{da_K}{dt} = \frac{\phi}{\tau_K} (a_{K,\infty} - a_K), \quad (9)$$

$$\frac{da_{\text{sd}}}{dt} = \frac{\phi}{\tau_{\text{sd}}} (a_{\text{sd},\infty} - a_{\text{sd}}), \quad (10)$$

$$\frac{da_{\text{sa}}}{dt} = \frac{\phi}{\tau_{\text{sa}}} (-\eta I_{\text{sd}} - \gamma a_{\text{sa}}), \quad (11)$$

where τ_{Na}, τ_K, τ_{sd}, and τ_{sa} are characteristic times. The parameter η serves for increasing calcium ion concentration following I_{sa}, while γ accounts for active elimination of intracellular Ca^{2+}. A second temperature-dependent scale factor is defined as

$$\phi = \phi_0^{\frac{(T - T_0)}{\tau_0}}. \quad (12)$$

The activation functions $a_{\text{Na},\infty}$, $a_{K,\infty}$, and $a_{\text{sd},\infty}$ depend on the membrane potential by the relations

$$a_{\text{Na},\infty} = \frac{1}{1 + \exp[-s_{\text{Na}}(V_i - V_{0\text{Na}})]}, \quad (13)$$

$$a_{K,\infty} = \frac{1}{1 + \exp[-s_K(V_i - V_{0K})]}, \quad (14)$$

$$a_{\text{sd},\infty} = \frac{1}{1 + \exp[-s_{\text{sd}}(V_i - V_{0\text{sd}})]}, \quad (15)$$

TABLE I. Parameter values of the neuronal dynamics model according to Ref. [21].

Membrane capacitance		$C_M = 1.0 \ \mu\text{F/cm}^2$		
Maximum conductances (mS/cm^2)				
$\bar{g}_{\text{Na}} = 1.5$	$\bar{g}_K = 2.0$	$\bar{g}_{\text{sd}} = 0.25$	$\bar{g}_{\text{sa}} = 0.4$	$\bar{g}_L = 0.1$
Characteristic times (ms)				
$\tau_{\text{Na}} = 0.05$	$\tau_K = 2.0$	$\tau_{\text{sd}} = 10$	$\tau_{\text{sa}} = 20$	
Reversal potentials (mV)				
$E_{\text{Na}} = 50$	$E_{\text{sd}} = 50$	$E_K = -90$	$E_{\text{sa}} = -90$	$E_L = -60$
$V_{0\text{Na}} = -25$	$V_{0K} = -25$	$V_{0\text{sd}} = -40$		
Other parameters				
$\rho_0 = 1.3$	$\phi_0 = 3.0$	$T_0 = 50 \,^{\circ}\text{C}$	$\tau_0 = 10$	$\eta = 0.012 \ \mu\text{A}$
$\gamma = 0.17$	$s_{\text{Na}} = 0.25$	$s_K = 0.25$	$s_{\text{sd}} = 0.09$	

where s_{Na}, s_K, and s_{sd} are constants and $V_{0\text{Na}}$, V_{0K}, and $V_{0\text{sd}}$ are activation voltages.

The parameter values used in our computer simulations are listed in Table I. The dynamics of an isolated neuron whose membrane potential follows the above system of equations $[\dot{V} = f_T(V)]$ depends on the temperature and, generally speaking, consists of a sequence of spikes which may or may not exhibit bursting behavior. We can identify the latter by computing, for a given temperature T, the interspike interval ISI. Figure 3 shows a bifurcation diagram for the interspike interval as a function of T.

Bursting behavior is characterized by the existence of two time scales: a fast time scale related to rapid spiking activity, followed by quiescent periods, or a slow time scale which we associate with bursts [50–55]. In terms of the bifurcation diagram, this means the existence of two bands with widely different average values of the ISI [21]. This happens for temperatures in the interval 37°–$39\,^{\circ}$C (the interval is indicated by dashed lines in Fig. 3). The original work of Huber and Braun has considered temperatures around $8\,^{\circ}C$, which is a value compatible with the kind of species it described (namely freshwater catfish and crayfish). We have altered the temperature constant T_0 to adapt the temperature range to the prevailing conditions in cat's brain [56].

A typical bursting event starts when a neuron fires a large number of fast spikes and ends with the ensuing
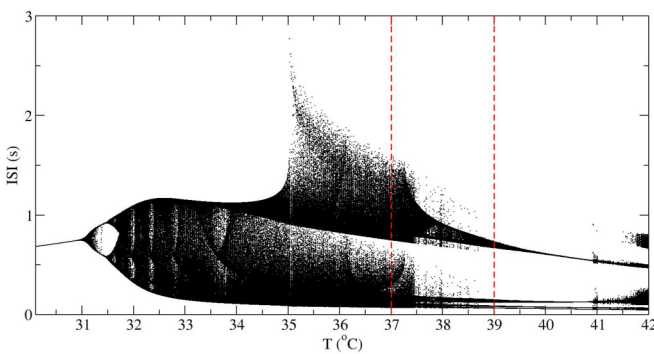

FIG. 3. (Color online) Bifurcation diagram for the interspike interval as a function of the temperature, for the Huber-Braun model, with numerical parameters as listed in Table I. The red dashed lines indicate the temperature range for which the neuron displays bursting behavior.

quiescent period. This is illustrated by the time evolution of the membrane potential of a single neuron, depicted in Fig. 4(a). The beginning of each burst has been found to be a local maximum of the recovery variable $U \equiv 1/I_{\text{isa}}$ [35]. It is possible to define a geometric bursting phase, which increases by 2π after each burst, even though the dynamics in each time scale is actually chaotic, as suggested by the bifurcation diagram of Fig. 3. Let t_k the time at which the kth bursting cycle begins [Fig. 4(b)]. The phase is obtained by a simple linear interpolation as [25]

$$\varphi(t) = 2\pi k + 2\pi \frac{t - t_k}{t_{k+1} - t_k}, \qquad (t_k < t < t_{k+1}), \qquad (16)$$

and increases monotonically with time. However, due to the chaotic evolution of the membrane potential V related to repetitive spiking, the interval $t_{k+1} - t_k$ differs for each burst. Hence we define an average bursting frequency,

$$\Omega = \frac{d\varphi}{dt} \doteq \lim_{t \to \infty} \frac{\varphi(t) - \varphi(0)}{t}, \qquad (17)$$

as the mean time rate of the phase evolution.

IV. DYNAMICS OF THE NEURONAL NETWORK

The neuronal network to be studied in this work consists of two levels: in the outer level the nodes are cortical areas and the links are the respective connections (axonal fibers). The architecture of these links is given by the corticocortical connectivity of the cat, represented by its weighted adjacency matrix A_{ij}, whose elements are depicted in Fig. 1. Each cortical area is a small-world network of neurons, obtained from the NW scheme with a given probability p.

Hence we consider S cortical areas, each of them with N neurons, i.e., the whole network has SN nodes (note that in Sec. II we denoted the number of neurons of the whole network by N). Each neuron will be identified by two labels $V_i^{(j)}$: the area j to which it belongs ($j = 1, 2, \dots S$) and its index i within the jth area ($i = 1, 2, \dots N$). The dynamics of the coupled neurons is described by the HB model, whose membrane equation is

$$C_M \frac{dV_i^{(j)}}{dt} = -I_{i,\text{Na}}^{(j)} - I_{i,K}^{(j)} - I_{i,\text{sd}}^{(j)} - I_{i,\text{sa}}^{(j)} - I_{i,L}^{(j)} + I_{i,\text{ext}}^{(j)}, \quad (18)$$

where the ionic currents for the jth neuron are given by Eqs. (2)–(6) and (8)–(15).
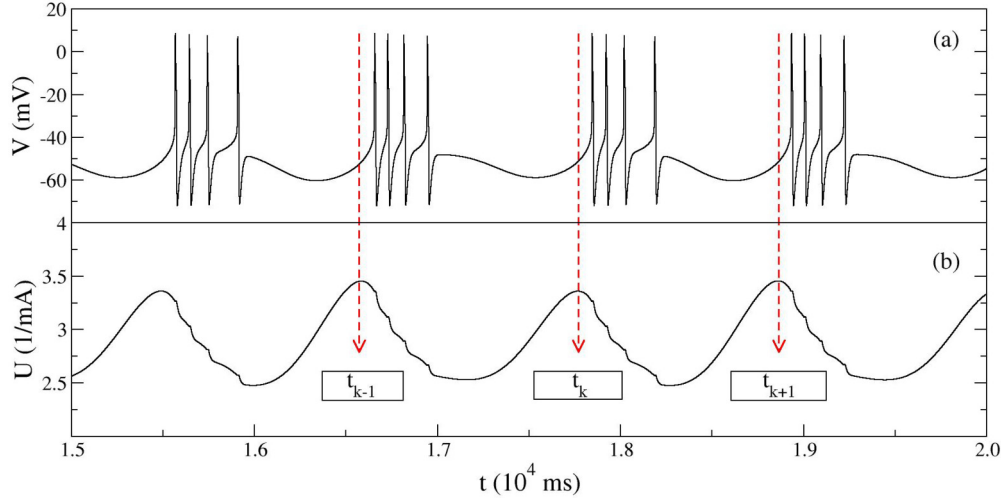
FIG. 4. (Color online) Time evolution of the (a) membrane potential V and (b) recovery variable $U = 1/I_{\text{isa}}$ indicating the times t_k at which it has a local maximum (for the definition of the bursting phase).

The coupling term for the jth neuron, denoted by $I_{i,\text{ext}}^{(j)}$, is represented by two synaptic currents of different nature: (i) an inner coupling, which stands for chemical synapses with a small-world connectivity within each area, and (ii) an outer coupling, by which the areas connect to each other through their corresponding mean potentials. The contribution of the inner coupling can be modelled as [56]

$$I_{i,\text{IN}}^{(j)} = g_{\text{IN}} \sum_{k=1}^{N} A_{ik}^{(j)} r_k^{(j)}(t)\big(V_{\text{syn}} - V_k^{(j)}\big), \qquad (19)$$

where g_{IN} is the inner coupling strength, or the maximal conductance of the synapse, $A_{ik}^{(j)}$ are the elements of the adjacency matrix for the jth area, V_{syn} is the synaptic reverse potential, and $r_k^{(j)}$ is the fraction of bound receptors of the kth neuron belonging to the jth area.

The latter variable undergoes a time evolution which can be described through a kinetic model devised by Destexhe and coworkers [56]. In a chemical synapse, after the arrival of an action potential at the presynaptic terminal, there is a release of neurotransmitter molecules (indicated by T) into the synaptic cleft, and these molecules bind to postsynaptic receptors.

Let $R_k^{(j)}$ and $T R_k^{(j)}$ denote the unbound and bound states of the postsynaptic receptors: the chemical synapse thus can be modelled by a kinetic process [56],

$$R_k^{(j)} + T_k^{(j)} \underset{[\beta]}{\overset{\alpha}{\rightleftharpoons}} T R_k^{(j)},$$

where α and β are the corresponding process rates, related to the characteristic rise and decay times, denoted as τ_r and τ_d, respectively. Moreover, let $r_k^{(j)}$ denote the fraction of bound receptors. The binding of the neurotransmitters to the postsynaptic receptor gates the opening of a ion channel, hence the total conductance of the synapse is $r_k^{(j)}$ times the maximal synapse conductance g_{IN}, in accordance with (19). As $r_k^{(j)}$ approaches unity, all channels reach the open state.

The time evolution of $r_k^{(j)}$, in a kinetic model, can be described by a master equation of the following form [57]

$$\frac{dr_k^{(j)}}{dt} = \alpha [T]_k^{(j)}\big(1 - r_k^{(j)}\big) - \beta r_k^{(j)}. \qquad (20)$$

In Ref. [56] it was supposed that the neurotransmitter concentration in the cleft ($[T]_k^{(j)}$) rises and falls so rapidly that it could be modelled by a square pulse, which enables one to solve (20) exactly. More complex models can be devised that take into account a dependence of $[T]_k^{(j)}$ with the membrane potential of the postsynaptic neurons $V_k^{(j)}$, such as [58]

$$\frac{dr_k^{(j)}}{dt} = \left(\frac{1}{\tau_r} - \frac{1}{\tau_d}\right)\frac{1 - r_k^{(j)}}{1 + \exp\big(-V_k^{(j)} + V_0\big)} - \frac{r_k^{(j)}}{\tau_d}, \quad (21)$$

where τ_r and τ_d are characteristic times and V_0 is a characteristic potential. The numerical values of the parameters used here are given in Table II. We suppose that their values are the same for each area. However, each cluster has a different adjacency matrix $A_{ik}^{(j)}$, since it describes a different realization of a small-world network obtained (from the NW scheme [48]).

The contribution of the outer coupling can also be described by a current density in the form

$$I_{\text{OUT}}^{(j)} = \frac{g_{\text{OUT}}}{S} \sum_{\ell=1}^{S} A_{j,\ell}^{(j)} M(j), \qquad (22)$$

with g_{IN} is the outer coupling strength (conductance), $A_{j,\ell}$ are the elements of the adjacency matrix of the cat cortex

TABLE II. Parameter values for the synaptic dynamics according to Ref. [22].

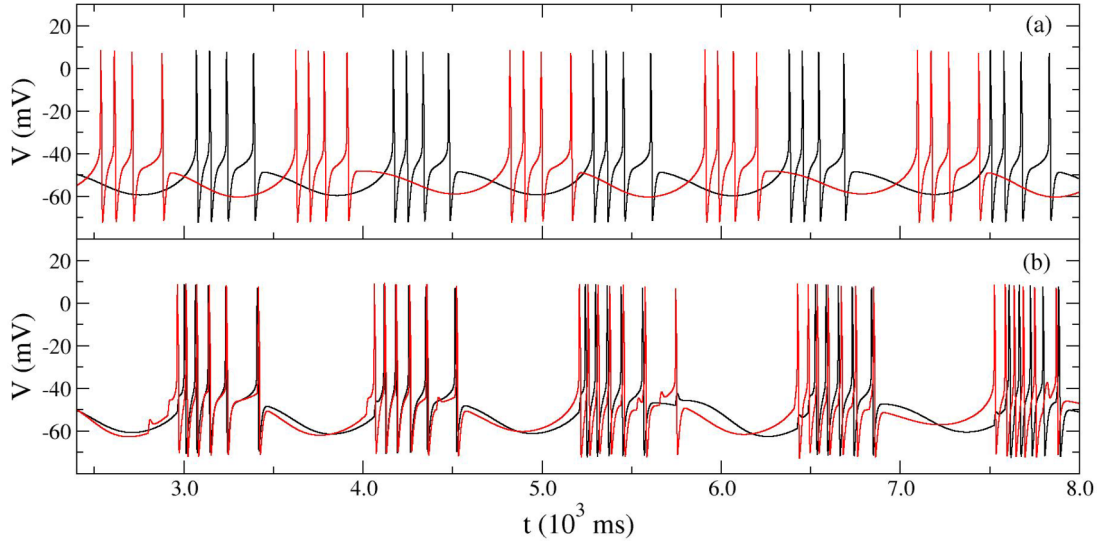| Characteristic times (ms)	
$\tau_r = 0.5$	$\tau_d = 8$
Reversal potentials (mV)	
$V_{\text{syn}} = 20$	$V_0 = -20$

FIG. 5. (Color online) Time evolution of the membrane potential of two selected neurons for (a) uncoupled and (b) coupled cases.

connectivity, and

$$M(j) = \frac{1}{N} \sum_{i=1}^{N} V_i^{(j)} \qquad (23)$$

is the mean field of the jth cluster, i.e., the cat matrix connects two cortical areas characterized collectively by their mean potentials. The total coupling current acting on the ith neuron belonging to the jth area is thus

$$I_{i,\text{ext}}^{(j)} = I_{i,\text{IN}}^{(j)} + I_{\text{OUT}}^{(j)}. \qquad (24)$$

Moreover, the values of the inner and outer coupling strengths, denoted by g_{IN} and g_{OUT}, respectively, are varied over an interval chosen as to always preserve a bursting behavior of the coupled neurons (a too-large coupling may drive the neuron off the bursting regime into an irregular spiking one).

The $6 \times S \times N = 82,408$ coupled differential equations were numerically integrated through a predictor-corrector scheme (fourth-order Adams method with a fixed step size of 0.01 and a tolerance less than 10^{-8} [59]) using GPU computing (a cluster of eight $K10$ and eight 2075 Tesla graphic cards) and CUDA [60]. As a result of the numerical integration we obtained $V_i^{(j)}(t)$ for each neuron, allowing the determination of the times t_k at which the bursting cycles occur for all of them. After a (very long) time interval we retrace the time series and compute, using Eq. (16), the time evolution of the corresponding phase, denoted φ_{ij}, for the ith neuron ($i = 1, 2, \ldots N$) belonging to the jth area ($j = 1, 2, \ldots S$).

V. BURSTING SYNCHRONIZATION

When, in an assembly of neurons, bursting begins at the same time, we have bursting synchronization irrespective of their spiking behavior within a given burst event. This is illustrated in Figs. 5(a) and 5(b), when we plot the time evolution of the membrane potential for two uncoupled and coupled neurons, respectively. This is obviously a weaker form of synchronization than complete synchronization, since the latter demands strict equality of potentials for all times. From a

dynamical point of view, since we assign a phase that increases by 2π at each burst event, we regard bursting synchronization as a kind of (chaotic) phase synchronization [25].

A. Order parameter

An assembly of neurons is said to exhibit bursting synchronization if their phases coincide for all times. This assembly can be, for example, a whole cluster or the entire network. Since bursting synchronization is an instance of phase synchronization, a useful quantitative diagnostic is provided by Kuramoto's order parameter z [61]. Let N be the number of neurons in a given cluster j. The complex order-parameter magnitude for the jth cluster is then defined as

$$R_j(t) = \left| \frac{1}{N} \sum_{i=1}^{N} e^{i\varphi_{ij}} \right|, \quad (j = 1, 2, \ldots S). \qquad (25)$$

If all neurons in a cluster are completely synchronized, then all the corresponding bursting phases coincide and thus the terms in (25) add coherently such that $R_j \to 1$. If, on the other hand, the neurons are completely nonsynchronized, then their bursting phases are totally uncorrelated and $R_j \to 0$. We may estimate that, in this case, $R \sim 1/\sqrt{N}$ for a finite network, since there will be a number of chance coincidences that eventually yield a nonzero sum. We choose the value of R_j at time $t = 3 \times 10^4$ ms, for which the transients have died out.

We can take the whole network into account in two ways: either we compute the (ensemble) average over all clusters,

$$R_{\text{mean}} = \frac{1}{S} \sum_{j=1}^{S} R_j, \qquad (26)$$

or we calculate the order-parameter magnitude for the whole network,

$$R_{\text{global}} = \left| \frac{1}{NS} \sum_{i=1}^{N} \sum_{j=1}^{S} e^{i\varphi_{ij}} \right|. \qquad (27)$$
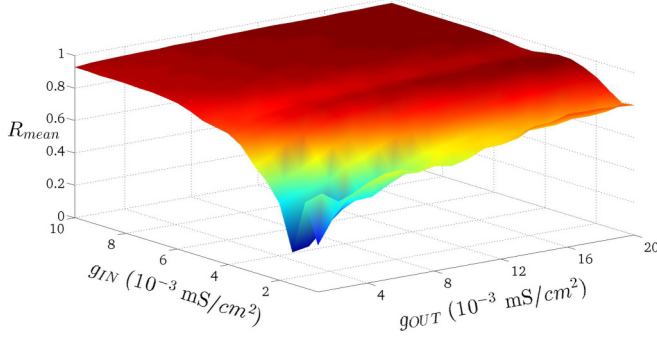
FIG. 6. (Color online) Cluster-averaged order parameter as a function of the two coupling parameters g_{IN} and g_{OUT} for a network of $S = 53$ clusters and $N = 256$ neurons *per* cluster. Each cluster is a small-world network obtained from the Newman-Watts scheme with probability $p = 0.01$. The clusters are connected through their mean fields using the cat cortical connectivity matrix.

FIG. 7. (Color online) Global order parameter as a function of the two coupling parameters g_{IN} and g_{OUT} for a network of $S = 53$ clusters and $N = 256$ neurons *per* cluster. Each cluster is a small-world network obtained from the Newman-Watts scheme with probability $p = 0.01$. The clusters are connected through their mean fields using the cat cortical connectivity matrix.

In Fig. 6 we plot the values of the clustered-averaged order parameter R_{mean} as a function of the two coupling parameters g_{IN} (inside each cluster) and g_{OUT} (connections among clusters). Considering, first, small values of g_{OUT}, say, between 1×10^{-3} and 4×10^{-3} mS/cm^2, such that the clusters are weakly connected among themselves, we find that the variation of R_{mean} with g_{IN} has the typical shape of a continuous phase transition: For small g_{IN} the clusters do not display phase synchronization, and so R_{mean} is correspondingly small. After a critical value of $g_{IN,\mathrm{cr}}$, however, the order parameter for each cluster (and their average) begins to increase according to a scaling law $R_{\mathrm{mean}} \sim (g_{IN} - g_{IN,\mathrm{cr}})^{\varpi}$, where $\varpi = 1/2$ for the Kuramoto model of phase oscillators. Since we have for each cluster a small-world network, the exponent ϖ is expected to differ, though.

As we increase the coupling among clusters ($g_{OUT} \neq 0$), the transition to synchronized behavior in the clusters continue to exist but with smaller values of the critical parameter $g_{IN,\mathrm{cr}}$, which is an effect of the increasing coupling strength caused by the outer network. Roughly speaking, the same scenario happens if we switch off the inner coupling and increase the outer coupling. In this case, however, the coupling between neurons is mediated by the mean fields of the clusters they belong to, and thus the effect is not so pronounced as before. Nevertheless, we have a transition scenario but with bumps and fluctuations that come from the indirect nature of the coupling.

For values of g_{OUT} between 1×10^{-3} and 4×10^{-3} mS/cm^2 the different cortical areas are weakly connected and, as we increase g_{IN}, we have a transition from a nonsynchronized to an almost synchronized state for each cluster. However, as long as g_{IN} is small enough there is no synchronization among different clusters. Moreover, small values of g_{OUT} favor the existence of a unique synchronized state as g_{IN} increases. This behavior can be observed in both Figs. 6 and 7, i.e., R_{mean} and R_{global} have similar behavior when g_{OUT} is relatively small.

The situation differs completely for $g_{OUT} > 14 \times 10^{-3}$ mS/cm^2: Due to the heterogeneity of the cat cortico-cortical connectivity matrix the synchronization of each area can be partially destroyed for some combinations of g_{IN} and

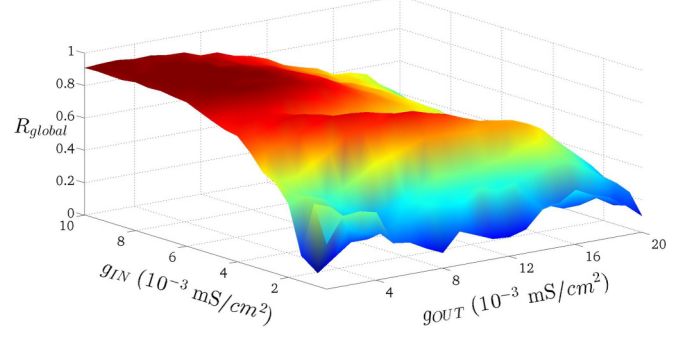g_{OUT}. For example, fixing g_{OUT} at a constant value, say, 1.8×10^{-4} mS/cm^2, and increasing g_{IN}, it happens that R_{global} initially increases (fast synchronization of all clusters) but a further increase of g_{IN} partially destroys this synchronized state. This cannot be readily observed in Fig. 7 because of the perspective of the figure, but there is a valley of low R_{global} for some combinations of g_{IN} and g_{OUT}. This point will be better clarified in the following discussion.

The difference between R_{mean} and R_{global} is particularly important when the bursting phases for the neurons in each cortical area synchronize at a given value, which differs for each area. Let us consider that the neurons at area 1 synchronize their bursting phases at a value, $\varphi_{11} = \varphi_{21} = \ldots = \varphi_{N1} = \Phi_1$. It follows that the order parameter corresponding to this area is $R_1 = 1$. Say that for area 2 the same happens, i.e., $\varphi_{12} = \varphi_{22} = \ldots = \varphi_{N2} = \Phi_2$, hence $R_2 = 1$, and so on. We thus have $R_{\mathrm{mean}} = (1/S) \sum R_j = 1$.

On the other hand, the global order parameter reads, in this case,

$$R_{\mathrm{global}} = \left| \frac{1}{S} \sum_{j=1}^{S} e^{i\,\Phi_j} \right|. \tag{28}$$

If $\Phi_1 = \Phi_2 = \ldots = \Phi_S$, then $R_{\mathrm{global}} = 1$, as expected. However, let us suppose that Φ_1, Φ_2, etc., are randomly and independently distributed. Then we get $R_{\mathrm{global}} = 0$. In general, for a given distribution of Φ_j, we have $R_{\mathrm{global}} \neq R_{\mathrm{mean}} = 1$, and the difference $\delta R = R_{\mathrm{mean}} - R_{\mathrm{global}}$ reflects the distribution.

Figure 8 exhibits the difference δR for the same parameters as considered in Figs. 6 and 7. Small values of δR occur for small g_{OUT}, irrespective of the values taken by g_{IN}. Hence when clusters are weakly coupled, both averages of the order parameter are similar ($R_{\mathrm{mean}} \approx R_{\mathrm{global}}$). The region where this difference is the most pronounced lies in an intermediate range of g_{OUT} and large g_{IN}. This coincides with the valley observed in Figs. 6 and 7 and is probably an effect of the dynamics of the coupled system.

The behavior of both R_{mean} and R_{global} as a function of g_{IN} within the above-mentioned valley can be observed in Figs. 9(a) and 9(b) for small and large values of g_{OUT}, respectively. In the former case, the behaviors of R_{mean} and
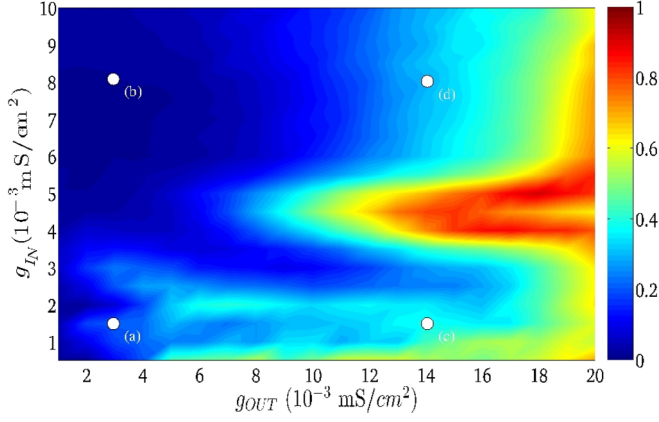
FIG. 8. (Color online) Difference (δR) between the cluster-averaged and the global order parameter as a function of the two coupling parameters g_{IN} and g_{OUT} for a network of $S = 53$ clusters and $N = 256$ neurons *per* cluster. Each cluster is a small-world network obtained from the Newman-Watts scheme with probability $p = 0.01$. The clusters are connected through their mean fields using the cat cortical connectivity matrix.

R_{global} are nearly the same, indicating that the entire network starts to synchronize at a unique state. In the latter (for strong g_{OUT}) the behaviors of R_{mean} and R_{global} differ and there is no longer a continuous transition. The vertical lines indicate the valley of nonsynchronized behavior among cortical areas.

Essentially what we have here is that, when a community of units display different averages of a certain quantity, the average of the averages differs from the overall average, as is well known from elementary statistics. The difference between both are basically due to the heterogeneity of the averages taken for all units (in our case, cortical areas).

B. Average field of the network

Another useful diagnostic of bursting synchronization is the average field of the network, which is the membrane potential after averaging over all the networks at a given time. If the neurons display synchronized bursting, it turns out that the network average field exhibits large-amplitude oscillations similar to those exhibited by the neurons themselves, due to the "constructive interference" of the potentials of each neuron. On the other hand, if the network is nonsynchronized at all, the average field experiences only low-amplitude and noiselike fluctuations, since there is a "destructive interference" among the neuron potentials [62].

In our model system, i.e., a clustered network with S cortical areas, each of them having N neurons, we define the average field in the jth area as

$$\langle V^{(j)} \rangle(t) = \frac{1}{N} \sum_{i=1}^{N} V_i^{(j)}(t), \qquad (j = 1, 2, \ldots S). \quad (29)$$

The corresponding variance (with respect to the spatial average at a particular time) is

$$\text{Var}(V^{(j)}(t)) = \frac{1}{N} \sum_{i=1}^{N} \left(V_i^{(j)}(t) - \langle V^{(j)} \rangle(t) \right)^2. \quad (30)$$

Since this variance depends on time, we can make a temporal mean within a time interval after transients have decayed

$$\overline{\text{Var}(V^{(j)})} = \lim_{T \to \infty} \frac{1}{T - T'} \int_{T'}^{T} dt \, \text{Var}(V^{(j)}(t)) \quad (31)$$

where we choose $T' = 24s$ and $T = 30s$

In the same way as we distinguished before between the average of averages taken for each cluster and the overall average of the network, we can also compute the overall average of the membrane potential,

$$\langle V_{\text{all}} \rangle(t) = \frac{1}{NS} \sum_{i=1}^{N} \sum_{j=1}^{S} V_i^{(j)}, \quad (32)$$
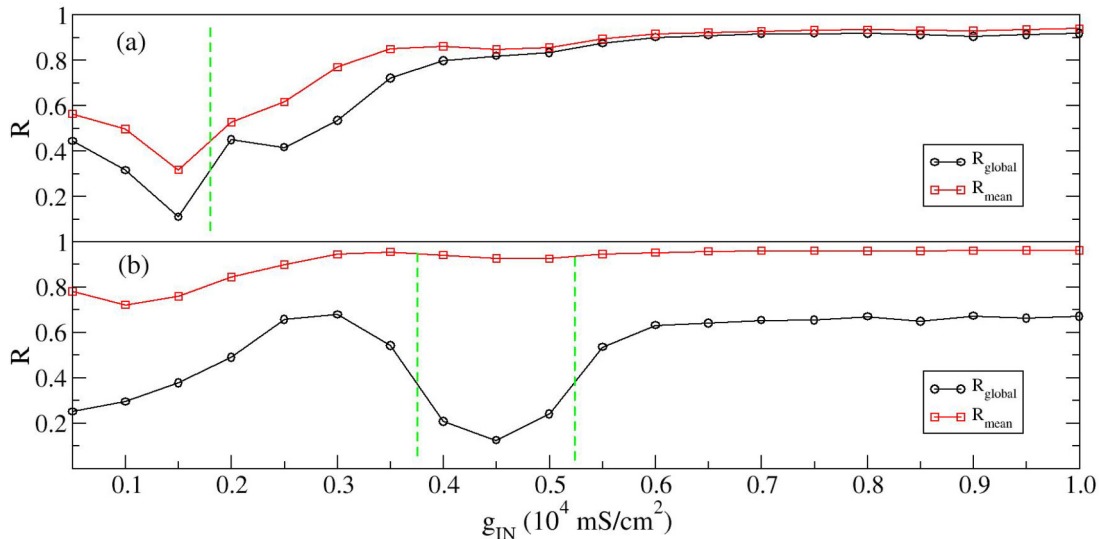

FIG. 9. (Color online) Dependence of R_{global} and R_{mean} with g_{IN} for (a) $g_{OUT} = 3 \times 10^{-3}$ mS/cm^2 and (b) 14×10^{-3} mS/cm^2. The remaining parameters are the same as in the previous figures.
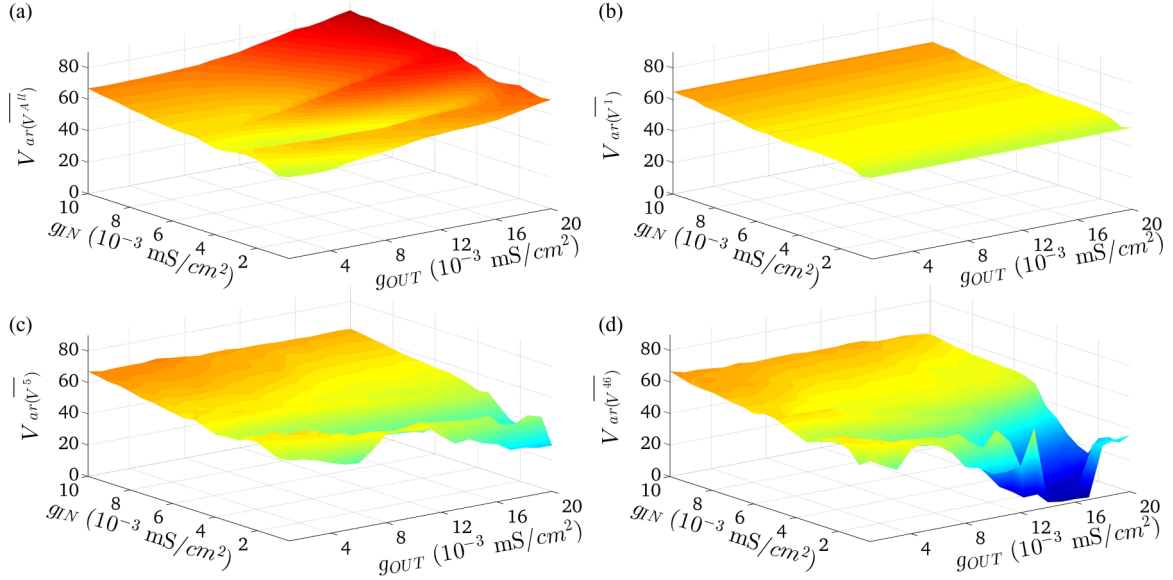
FIG. 10. (Color online) Variances of the average membrane potential as a function of the coupling parameters g_{IN} and g_{OUT} for a network of $S = 53$ clusters and $N = 256$ neurons *per* cluster. Each cluster is a small-world network obtained from the Newman-Watts scheme with probability $p = 0.01$. The clusters are connected through their mean fields using the cat cortical connectivity matrix. (a) Overall variance and variances for cluster numbers 1 (b), 5 (c), and 46 (d).

where $V_i^{(j)}$ denotes the membrane potential of the ith neuron belonging to the jth cluster. The variance with respect to this average (at a given time) can be used to quantify the amount of bursting synchronization taken the network as a whole,

$$\text{Var}(V_{\text{all}})(t) = \frac{1}{NS} \sum_{i=1}^{N} \sum_{j=1}^{S} \left(V_i^{(j)}(t) - \langle V_{\text{all}} \rangle(t) \right)^2. \quad (33)$$

The corresponding temporal mean of this quantity is

$$\overline{\text{Var}(V_{\text{all}})} = \lim_{T \to \infty} \frac{1}{T - T'} \int_{T'}^{T} dt \, \text{Var}(V_{\text{all}})(t). \quad (34)$$

The dependence of the latter quantity with the internal and external coupling strengths is depicted in Fig. 10(a). We find that if the areas are not coupled ($g_{OUT} = 0$), then we still see a passage from a nonsynchronized to a synchronized bursting as the internal coupling g_{IN} increases. However, it is not possible to infer from the increase of the variance that this is actually a transition-like phenomenon that would justify the use of the order parameter, which is a more accurate way to determine the loss of synchronization. The same increase of variance is observed for coupled areas ($g_{OUT} \neq 0$), and the shape of the surface in the parameter space is quite smooth due to the overall character of the average taken from Eq. (32).

The variances for each cluster, taken separately from the other ones and obtained from (30), are depicted in Figs. 10(b) to 10(d) for the areas numbered as $j = 1, 5,$ and 46, respectively, picked up to display examples of how the behavior in each cluster can differ markedly from the network as a whole. For example, area 1 apparently does not change its synchronized transition for different values of g_{OUT}, i.e., this area is barely affected by the external coupling of the community. On the other hand, area $j = 46$ has a widely different behavior, indicating that it is strongly affected by the interaction among areas.

In Figure 11(b) we plot the time evolution of the average for each cluster, $\langle V^{(j)} \rangle(t)$, where $j = 1, 2, \ldots S$ for $g_{IN} = 0.0015$ mS/cm^2 and $g_{OUT} = 0.003$ mS/cm^2. This case corresponds to weak coupling, both internally and externally to the clusters, and has been indicated by the letter (a) in Fig. 8. Although in the figure we show results for time intervals up to 2000 ms, such states are stationary since we have extended the numerical simulations for much longer time intervals without finding major changes. We see that for nearly all clusters the average potential displays low-amplitude oscillations, indicating nonsynchronized behavior. A noteworthy point is the increase of the variance from cluster number 35 to 53, suggesting that for these clusters the interactions are stronger such that there is a slight reduction of the overall effect of suppression of synchronization. In fact, if we inspect the corticocortical connectivity map in Fig. 1, we see that the density of connections is larger for these clusters.
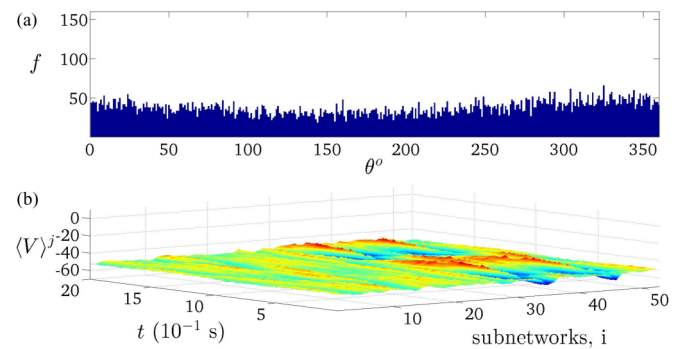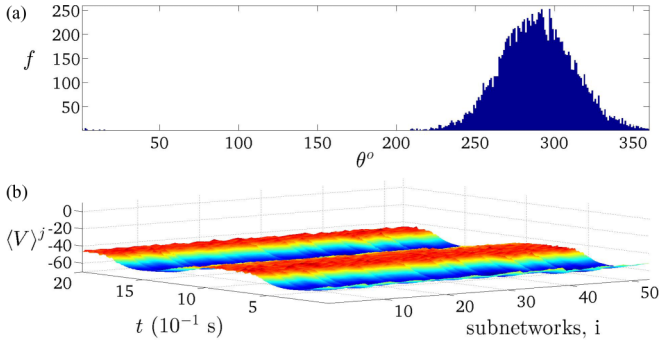

FIG. 11. (Color online) (a) Histogram of the bursting phases φ_{ij} of the ith neuron belonging to the jth cluster at a fixed time and (b) variance of the jth cluster as function of time. The coupling parameters are $g_{IN} = 0.0015$ mS/cm^2 and $g_{OUT} = 0.003$ mS/cm^2. Other parameters are the same as in the previous figures.

FIG. 12. (Color online) (a) Histogram of the bursting phases φ_{ij} of the ith neuron belonging to the jth cluster at a fixed time and (b) variance of the jth cluster as function of time. The coupling parameters are $g_{\text{IN}} = 0.008$ mS/cm^2 and $g_{\text{OUT}} = 0.003$ mS/cm^2. Other parameters are the same as in the previous figures.

Nonsynchronized behavior, in this case, means that practically all values of the phase $\varphi_{ij} \in [0, 2\pi)$ would be visited by the bursting neurons. This is confirmed by Fig. 11(a), where we plot a histogram of the number of neurons with a given value of the phase at fixed time, which is a numerical approximation for a probability distribution function $P(\varphi)$, which is broadly distributed in the interval $[0, 2\pi)$, as expected for weakly correlated clusters.

Now we increase the value of g_{IN} and keep g_{OUT} unchanged (Fig. 12), which corresponds to a strong internal and weak external coupling (it has been indicated by letter (b) in Fig. 8). In Fig. 12(b) we observe that essentially all clusters exhibit large-amplitude oscillations of the average potential. Moreover, these oscillations are mutually correlated (they have nearly the same phase and period), meaning that the clusters are strongly synchronized. In fact, the histogram of Fig. 12(a) indicates a clear preference of the neurons for bursting phases belonging to an interval between $240°$ and $360°$.

A different scenario is observed in Fig. 13, for which g_{IN} is small but g_{OUT} is large (indicated by letter (c) in Fig. 8). The time evolution of the averages $\langle V^{(j)} \rangle$ varies widely according to the cluster [Fig. 13(b)], and we observe tendencies to both complete phase synchronization and partial
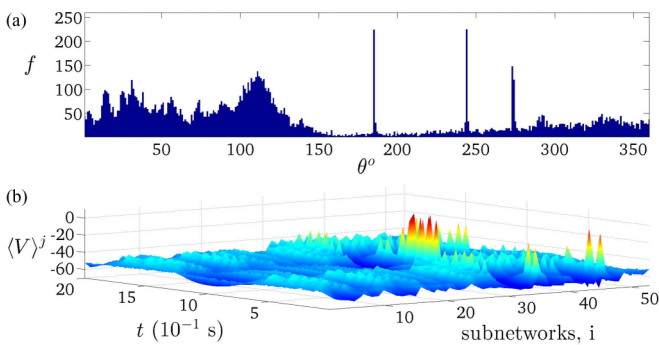

FIG. 13. (Color online) (a) Histogram of the bursting phases φ_{ij} of the ith neuron belonging to the jth cluster at a fixed time and (b) variance of the jth cluster as function of time. The coupling parameters are $g_{\text{IN}} = 0.0015$ mS/cm^2 and $g_{\text{OUT}} = 0.014$ mS/cm^2. Other parameters are the same as in the previous figures.
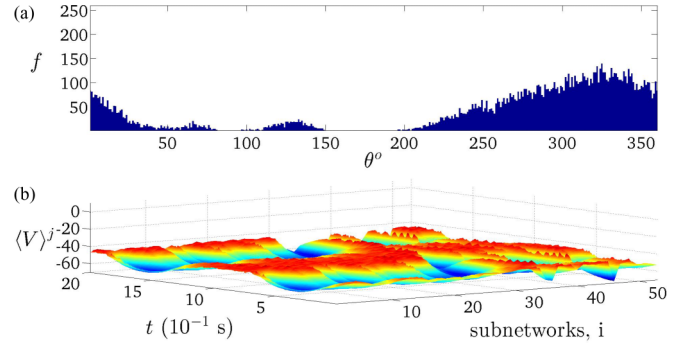

FIG. 14. (Color online) (a) Histogram of the bursting phases φ_{ij} of the ith neuron belonging to the jth cluster at a fixed time and (b) variance of the jth cluster as function of time. The coupling parameters are $g_{\text{IN}} = 0.008$ mS/cm^2 and $g_{\text{OUT}} = 0.014$ mS/cm^2. Other parameters are the same as in the previous figures. (a) Histogram and (b) variance.

synchronization. This is confirmed by the histogram shown in Fig. 13(a), which has sharp peaks at some angles (for a complete synchronization) and broader peaks indicating partial synchronization.

Finally, the case when both g_{IN} and g_{OUT} take large values [indicated by letter (d) in Fig. 8] is depicted in Fig. 14. From the time evolution of the cluster averages [Fig. 14(a)] and the histogram of the phases [Fig. 14(b)] we conclude that many (but not all) clusters are mutually partially synchronized, presenting a wide bell-shaped probability distribution of phases but without narrow peaks at some angles, as in the previous case.

VI. CONCLUSIONS

Complex networks are often organized as assemblies of smaller communities. These communities interact with each other in a weaker fashion, when compared with a strong interaction within those communities. This clustered structure is found in neuronal networks in both anatomic and functional levels. One example of a clustered neuronal network is the cat corticocortical connectivity map, in which the units—the cortical areas—are in fact clusters with a large number of individual neurons. We have used in this paper small-world networks to describe these clusters, obtained from a regular chain by randomly adding shortcuts with a given probability. These clusters interact with each other according to the corticocortical connectivity map described in the literature from experimental data.

Clustered networks are expected to contribute to complex dynamics, especially when the neurons themselves undergo a chaotic time evolution. We choose a mathematical model of bursting neurons to emulate this situation and study effects of synaptic (chemical) coupling on the dynamics of the entire network as well as of its constituent clusters. One of the dynamical features displayed by coupled bursting neurons is synchronization of their bursting activity: Even though the neuronal spiking may be uncorrelated, neuron bursts begin approximately at the same time.

We assign a phase to each bursting cycle, such that bursting synchronization is essentially an example of chaotic phase

synchronization of nonlinear oscillators. Synchronization of bursting neurons of a given brain region is thought to be related to some neurological disorders (pathological rhythms like essential tremor, epilepsy, and Parkinson's disease). Once this synchronization happens in a limited number of neurons, say, in a given cluster, is it possible that a larger portion of the brain also becomes synchronized? If a number of areas are synchronized at different levels, what could be the overall effect in terms of the entire network?

Such questions can be addressed in the context of the numerical solution of the mathematical model we considered in this work. We choose the parameters to be varied the synaptic conductances within each area (g_{IN}) and among different clusters (g_{OUT}). As a general trend, the larger the values of both the more synchronized the entire network. In fact, the effect of g_{IN} is more pronounced than g_{OUT} to achieve the same effect. Hence the internal cluster dynamics influences the overall result more than the intercluster coupling.

It may well happen that a number of clusters are synchronized at different levels, which results in a nonsynchronized behavior, when considered from a global point of view. This clearly differs, however, from a situation when all clusters are themselves nonsynchronized. We have defined, to distinguish between these situations, suitable quantities based on the order parameters computed for both the entire network and for the average taken over various cortical areas. We have found that

large values of this quantity are observed for intermediate values of g_{IN} and large values of g_{OUT}. The reason for this is still unclear but probably results from the dynamics of the coupled system.

The same observations can be made from the analysis of the variance of the mean field related to the whole network and the mean over the various clusters belonging to it. However, the dynamical mechanism leading to these partial synchronization phenomena is still to be described. In our system the complexity of the model equations prevent such an analytical treatment, but we hope that this may be feasible in simpler systems like the Kuramoto model of globally coupled oscillators. A bursting neuron can be reduced to an autonomous phase oscillator in such a way that the Kuramoto model is a toy model to investigate the partial synchronization phenomena existing in clustered neuronal networks.

[1] J. G. Nicholls, A. R. Martin, B. G. Wallace, and P. A. Fuchs, *From Neuron to Brain*, 4th ed. (Sinauer, Sunderland, MA, 2001).

[2] E. R. Kandel, J. H. Schwartz, and T. M. Jessell, *Principles of Neural Science*, 4th ed. (McGraw-Hill, New York, 2000).

[3] C. C. Hilgetag and M. Kaiser, in *Lectures in Supercomputational Neuroscience: Dynamics in Complex Brain Networks*, edited by P. B. Graben, C. Zhou, M. Thiel, and J. Kurths (Springer, Berlin, 2008).

[4] M. F. Bear, B. W. Connors, and M. A. Paradisio, *Neuroscience: Exploring the Brain*, 3rd ed. (Lippincott Williams & Wilkins, Philadelphia, 2007).

[5] J. W. Scannell and M. P. Young, Curr. Biol. **3**, 191 (1993).

[6] J. W. Scannell, C. Blakemore, and M. P. Young, J. Neurosci. **15**, 1463 (1995).

[7] J. W. Scannell, G. A. P. C. Burns, C. C. Hilgetag, M. A. O'Neil, and M. P. Young, Cereb. Cortex **9**, 277 (1999).

[8] G. Zamora-López, C. Zhou, and J. Kurths, Front. Neurosci. **5**, 83 (2011).

[9] G. Zamora-López, C. Zhou, and J. Kurths, Front. Neuroinform. **4**, 1 (2010).

[10] E. L. Lameu, C. A. S. Batista, A. M. Batista, K. Iarosz, R. L. Viana, S. R. Lopes, and J. Kurths, Chaos **22**, 043149 (2012).

[11] H. D. I. Abarbanel, M. I. Rabinovich, A. Selverston, M. V. Bazhenov, R. Huerta, M. M. Sushchik, and L. L. Rubchinskii, Phys. Uspekhi **39**, 337 (1996).

[12] S. Coombes and P. C. Bressloff (eds.) *Bursting: The Genesis of Rhythm in the Nervous System* (World Scientific Press, Singapore, 2005).

[13] E. M. Izhikevich, *Dynamical Systems in Neuroscience: The Geometry of Excitability and Bursting* (The MIT Press, Cambridge, MA, 2007).

[14] W. Gerstner and W. M. Kistler, *Spiking Neuron Models* (Cambridge University Press, New York, 1999).

[15] A. L. Hodgkin and A. F. Huxley, J. Physiol. **117**, 500 (1952).

[16] H. A. Braun, M. T. Huber, M. Dewald, K. Schäfer, and K. Voigt, Int. J. Bifurcat. Chaos **8**, 881 (1998).

[17] W. Braun, B. Eckhardt, H. A. Braun, and M. Huber, Phys. Rev. E **62**, 6352 (2000).

[18] H. A. Braun, M. T. Huber, N. Anthes, K. Voigt, A. Neiman, X. Pei, and F. Moss, Biosystems **62**, 99 (2001).

[19] H. A. Braun, M. Dewald, K. Schäfer, K. Voigt, X. Pei, K. Dolan, and F. Moss, J. Comput. Neurosci. **7**, 17 (1999).

[20] K. Schäfer, H. A. Braun, R. C. Peters, and F. Bretschneider, Pflügers Arch. Eur. J. Physiol. **429**, 378 (1995).

[21] U. Feudel, A. Neiman, X. Pei, W. Wojtenek, H. Braun, M. Huber, and F. Moss, Chaos **10**, 231 (2000).

[22] Y. Hao, Y. Gong, L. Wang, X. Ma, and C. Yang Chaos, Solit. Fract. **44**, 260 (2011).

[23] S. Postnova, K. Voigt, and H. A. Braun, J. Biol. Phys. **33**, 129 (2007).

[24] A. Arenas, A. Díaz-Guilerac, J. Kurths, Y. Moreno, and C. Zhou, Phys. Rep. **469**, 93 (2008).

[25] M. V. Ivanchenko, G. V. Osipov, V. D. Shalfeev, and J. Kurths, Phys. Rev. Lett. **93**, 134101 (2004).

[26] C. A. S. Batista, E. L. Lameu, A. M. Batista, S. R. Lopes, T. Pereira, G. Zamora-López, J. Kurths, and R. L. Viana, Phys. Rev. E **86**, 016211 (2012).

[27] A. M. Batista, S. E. de S. Pinto, R. L. Viana, and S. R. Lopes, Physica A **322**, 118 (2003).

[28] E. Barreto, B. R. Hunt, E. Ott, and P. So, Phys. Rev. E **77**, 036107 (2008).

[29] E. Montbrio, J. Kurths, and B. Blasius, Phys. Rev. E **70**, 056125 (2004).

[30] A. Pikovsky and M. Rosenblum, Phys. Rev. Lett. **101**, 264103 (2008).

[31] P. S. Skardal and J. G. Restrepo, Phys. Rev. E **85**, 016208 (2012).

[32] D. Anderson, A. Tenzer, G. Barlev, M. Girvan, T. M. Antonsen, and E. Ott, Chaos **22**, 013102 (2012).

[33] O. Sporns and J. D. Zwi, Neuroinformatics **2**, 145 (2004).

[34] D. S. Bassett and E. Bullmore, Neuroscientist **12**, 512 (2006).

[35] C. A. S. Batista, R. L. Viana, F. A. S. Ferrari, S. R. Lopes, A. M. Batista, and J. C. P. Coninck, Phys. Rev. E **87**, 042713 (2013).

[36] A. Beuter, M. S. Titcombe, F. Richer, C. Gross, and D. Guehl, Thalamus Relat. Syst. **1**, 203 (2001).

[37] M. Steriade, D. A. McCormick, and T. J. Sejnowski, Science **262**, 679 (1993).

[38] L. B. Good, S. Sabesan, S. T. March, K. Tsakalis, D. Treiman, and L. Iasemidis, Int. J. Neural Syst. **19**, 173 (2009).

[39] A. Beuter and M. S. Titcombe, Brain Cognition **53**, 190 (2003).

[40] M. S. Titcombe, L. Glass, D. Guehl, and A. Beuter, Chaos **11**, 766 (2001).

[41] J. Y. K. Lee and D. Kondziolka, J. Neurosurg. **103**, 400 (2005).

[42] P. Bain, T. Aziz, X. Liu and D. Nandi (eds.), *Deep Brain Stimulation* (Oxford University Press, Oxford, 2009).

[43] R. Albert and A.-L. Barabási, Rev. Mod. Phys. **74**, 47 (2002).

[44] D. J. Watts, *Small Worlds* (Princeton University Press, Princeton, NJ, 2000).

[45] P. Erdös and A. Rényi, Publicat. Mathematicae **6**, 290 (1959).

[46] L. R. Varshney, B. L. Chen, E. Paniagua, D. H. Hall, and D. B. Chklovskii, PLOS Comput. Biol. **7**, e1001066 (2011).

[47] D. J. Watts and S. H. Strogatz, Nature **393**, 440 (1998).

[48] M. E. J. Newman and D. J. Watts, Phys. Rev. E **60**, 7332 (1999).

[49] P. R. Shorten and D. Wall, Bull. Math. Biology **62**, 695 (2000).

[50] H. Degn, A. V. Holden, and L. F. Olsen (eds.), *Chaos in Biological Systems* (Plenum Press, New York, 1987).

[51] L. Glass and M. C. Mackey, *From Clocks to Chaos* (Princeton University Press, Princeton, NJ, 1988).

[52] T. Elbert, W. J. Ray, Z. J. Kowalik, J. E. Skinner, K. E. Graf, and N. Birbaumer, Physiol. Rev. **74**, 1 (1994).

[53] M. W. Slutzky, P. Cvitanovic, and D. L. Mogul, Annals Biomed. Engineering **29**, 607 (2001).

[54] H. Korn and P. Faure, C. R. Biol. **326**, 787 (2003).

[55] J. N. Hayward and M. A. Baker, Brain Res. **16**, 417 (1969).

[56] A. Destexhe, Z. F. Mainen, and T. J. Sejnowski, Neural Comput. **6**, 14 (1994).

[57] M. Perc, Biophys. Chem. **141**, 175 (2009).

[58] C. Morris and H. Lecar, Biophys. J. **35**, 193 (1981).

[59] A. C. Hindmarsh, in *ODEPACK, A Systematized Collection of ODE Solvers*; in Scientific Computing, edited by R. W. Stepleman *et al.* (North-Holland, Amsterdam, 1983), p. 55; L. R. Petzold, Siam J. Sci. Stat. Comput. **4**, 136 (1983).

[60] http://www.nvidia.com/object/cuda_home_new.html.

[61] Y. Kuramoto, *Chemical Oscillations, Waves and Turbulence* (Dover, New York, 2003).

[62] M. G. Rosenblum and A. S. Pikovsky, Phys. Rev. Lett. **92**, 114102 (2004).